

# Capacity Maximization Pattern Design for Reconfigurable MIMO Antenna Array

Haonan Wang, *Student Member, IEEE*, Ang Li, *Senior Member, IEEE*,

Ya-Feng Liu, *Senior Member, IEEE*, Qibo Qin, *Fellow, IEEE*, Lingyang Song, *Fellow, IEEE*, and Yonghui Li, *Fellow, IEEE*

**Abstract**—Multi-functional and reconfigurable multiple-input multiple-output (MR-MIMO) can provide performance gains over traditional MIMO by introducing additional degrees of freedom. In this paper, we focus on the capacity maximization pattern design for MR-MIMO systems. Firstly, we introduce the matrix representation of MR-MIMO, based on which a pattern design problem is formulated. To further reveal the effect of the radiation pattern on the wireless channel, we consider pattern design for both the single-pattern case where the optimized radiation pattern is the same for all the antenna elements, and the multi-pattern case where different antenna elements can adopt different radiation patterns. For the single-pattern case, we show that the pattern design is equivalent to a redistribution of power among all scattering paths, and an eigenvalue optimization based solution is obtained. For the multi-pattern case, we propose a sequential optimization framework with manifold optimization and eigenvalue decomposition to obtain near-optimal solutions. Numerical results validate the superiority of MR-MIMO systems over traditional MIMO in terms of capacity, and also show the effectiveness of the proposed solutions.

**Index Terms**—Multifunctional and reconfigurable antennas, reconfigurable MIMO, pattern design, sequential optimization, manifold optimization.

## I. INTRODUCTION

MULTIPLE-input multiple-output (MIMO) techniques have received extensive research attention due to their diversity and multiplexing gain over single-input single-output (SISO) systems [1]. This includes point-to-point (P2P) MIMO systems where both the transmitter and the receiver are equipped with multiple antennas to improve the system capacity via transmitting multiple data streams simultaneously. The benefits further extend to multi-user MIMO (MU-MIMO) systems, where a multi-antenna transmitter serves a set of single-

antenna or multi-antenna users simultaneously for spatial multiplexing. More recently, employing reconfigurable antennas at wireless transceivers is shown to offer additional performance gains over traditional antennas with fixed radiation characteristics [2]. Therefore, multi-functional and reconfigurable MIMO (MR-MIMO) techniques are seen as potential candidates for 5G and beyond communication systems [3].

Reconfigurable antennas form a special class of antennas which can be configured to operate with different frequency bands, different polarizations or radiation patterns [4], [5]. Among different types of reconfigurable antennas, the pattern reconfigurability which is the focus of this paper, can improve the degrees of freedom (DoFs) in the signal directions so that the ability of interference suppression and energy saving can be further enhanced, while the frequency reconfigurability can reduce the interference from other wireless signals operating in the same frequency band. The polarization reconfigurability can switch between left-handed circular polarization (LHCP) and right-handed circular polarization (RHCP) to reduce the polarization mismatch and employ the polarization coding. Thanks to the development of micro-electromechanical system (MEMS) switching, semi-conductor switches, liquid metals, etc., various types of reconfigurable antennas have been designed based on variable reactive loading, parasitic tuning and material modifications [6]. The applications of reconfigurable antennas in MIMO systems have been studied in some pioneering works in [7]–[9]. For example in [7], the throughput gain provided by reconfigurable antennas was analyzed mathematically and it was shown that reconfiguration patterns can be seen as additional channel realizations. As one of the earliest realizations of MR-MIMO, compact parasitic arrays in the form of electronically steerable parasitic antenna radiators (ESPARs) utilized the mutual coupling to provide additional DoFs with only one active RF chain [8], [9]. By employing tunable loads instead of fixed loads at each parasitic antenna element, the mutual coupling could be controlled so that different radiation patterns could be formed [9].

Pattern reconfigurable MIMO can provide diversity in antenna directivity at the same operating frequency, and there already existed a considerable number of methods to realize pattern reconfigurable MIMO [10]. A common method was to use a switching circuit to feed a sector array such that only one array element was executed at each timeslot [11], [12]. By replacing the switching circuit with a reconfigurable power divider, bidirectional and omnidirectional patterns would be obtained [13]–[15]. Meanwhile, other methods for realizing pattern reconfiguration include choosing different radiation

Haonan Wang and Ang Li are with the School of Information and Communications Engineering, Faculty of Electronic and Information Engineering, Xi'an Jiaotong University, Xi'an, Shaanxi, China, and are also with The State Key Laboratory of Integrated Services Networks, Xidian University, Xi'an, Shaanxi, China (e-mail: ang.li.2020@xjtu.edu.cn, whn8215858@stu.xjtu.edu.cn).

Ya-Feng Liu is with the State Key Laboratory of Scientific and Engineering Computing, Institute of Computational Mathematics and Scientific/Engineering Computing, Academy of Mathematics and Systems Science, Chinese Academy of Sciences, Beijing 100190, China (e-mail: yafliu@lsec.cc.ac.cn).

Qibo Qin is with Wireless Network RAN Research Department, Shanghai Huawei Technologies Co. Ltd., Shanghai 201206, China (e-mail: qin-qibo1@huawei.com).

Lingyang Song is with the School of Electrical Engineering and Computer Science, Peking University, Beijing 100871, China (e-mail: lingyang.song@pku.edu.cn).

Yonghui Li is with the School of Electrical and Information Engineering, The University of Sydney, Sydney, NSW 2006, Australia (e-mail: yonghui.li@sydney.edu.au).

units, changing the characteristic modes of radiators, etc., [16], [17]. Because of the ability to increase the signal transmission distance and quality, pattern reconfigurable MIMO has been mostly promising in the region of surveillance and tracking. For example, [18] designed a high-gain pattern reconfigurable MIMO antenna array to increase the power efficiency in wireless handheld terminals. What's more, [19] proposed an approach to analyze the characterization of pattern reconfigurable antennas designed for MIMO systems. It revealed that pattern reconfigurable MIMO can redirect the signal to intended users so that the energy efficiency can be increased and the communication coverage can be extended.

The performance benefits of MR-MIMO mainly come from the additional DoFs, and the exploitation of such additional DoFs is mainly accomplished through the effective optimal mode selection scheme. Currently, several applications of MR-MIMO have been promoted in areas such as MIMO transmission [20], target detection and tracking [21], direction of arrival (DoA) estimation [22], [23]. In [20], the additional efficient channels generated by MR-MIMO expanded the users scheduling region, which would further improve the performance. A joint user and antenna mode selection algorithm based on determinant pairing scheduling was proposed, and a greedy low-complexity iterative selection scheme was further designed. [21] discussed the application of MR-MIMO in the field of target detection and tracking, and proposed a Bayesian cognitive target tracking technique, which minimized the Cramér-Rao lower bound (CRLB) of the DoA parameters through an adaptive selection of the reconfigurable antennas' modes. With respect to the DoA estimation for MR-MIMO, the traditional estimation technique was combined with the mode selection scheme and an improved performance could be achieved [22], [23].

Despite the above studies, there are still two challenges preventing the practical application of MR-MIMO. On one hand, the mode selection mechanism brings unacceptable channel estimation overhead. The channel prediction based on the correlation among the pattern modes [24] and the effective mode selection scheme based on reinforcement learning (RL) [25]–[29] are the major solutions to this issue currently. On the other hand, the physical mechanism of how the radiation pattern of MR-MIMO affects the channel has not been revealed, and it is not clear how to design the optimal radiation pattern for capacity maximization in MR-MIMO systems, which is the focus of this paper.

In this paper, we study the capacity maximization pattern design for MR-MIMO systems. We firstly introduce the matrix representation framework of MR-MIMO and further formulate a pattern design problem. In order to fully reveal the effect of the reconfigurable radiation pattern on the wireless channel, we consider both the single-pattern case where the optimized radiation pattern is the same for all the antenna elements, and the multi-pattern case where each antenna element can adopt different radiation pattern. The main contributions of this paper are summarized as follows:

- We obtain a matrix representation formulation of the MIMO channel with pattern reconfigurability. The effect of the reconfigurable pattern is described as a pattern

sampling matrix, which reveals that the pattern affects the channel by redistributing the channel gains in the direction of the scattering paths. The optimal pattern design problem aimed at maximizing the capacity is formulated.

- In the single-pattern case, the requirement that all the antennas adopt the same radiation pattern results into the non-convexity of the relaxed capacity maximization pattern design problem. In order to solve the problem with low complexity and reveal the design principle of the pattern design problem, we transform the problem and show that the pattern design is equivalent to redistributing power among different scattering paths, based on which an eigenvalue optimization based power allocation scheme is derived.
- For the multi-pattern case, a sequential optimization framework (SOF) is proposed as a sub-optimal scheme. In order to simplify the problem, we transform the design of the correlation modification matrix into a sequential optimization problems on correlation modification vectors, where a criterion to determine their sequences to be optimized is presented. The subproblem for each vector optimization is solved via manifold optimization and eigenvalue decomposition.
- Numerical results clearly illustrate the power redistribution process of MR-MIMO in the single-pattern case and the correlation modification process in the multi-pattern case. In addition, numerical results also demonstrate the superiority of MR-MIMO with near-optimal pattern design over traditional MIMO systems in terms of capacity.

The rest of the paper is organized as follows. In Section II, we describe the system model of MR-MIMO. In Section III, the matrix representation for MR-MIMO is derived, and an optimization problem of the optimal pattern design is formulated. In Section IV, pattern design algorithms are proposed for both single-pattern and multi-pattern MR-MIMO. Simulation results are provided in Section IV, and the paper is concluded in Section V with future directions.

Notations:  $a$ ,  $\mathbf{a}$ , and  $\mathbf{A}$  denote scalar, vector and matrix, respectively.  $(\cdot)^*$ ,  $(\cdot)^T$ ,  $(\cdot)^H$  and  $\text{Tr}(\cdot)$  denote conjugate, transposition, conjugate transposition and trace of a matrix, respectively.  $\text{vec}(\cdot)$  denotes the vectorization operator and  $\text{diag}(\cdot)$  transforms a vector into a diagonal matrix.  $\langle \cdot, \cdot \rangle$  denotes the inner product of two vectors, i.e.,  $\langle \mathbf{a}, \mathbf{b} \rangle = \mathbf{a}^H \mathbf{b}$  for complex vectors  $\mathbf{a}$  and  $\mathbf{b}$ . Frobenius norm of a matrix is denoted by  $\|\cdot\|_F$ .  $\mathbf{I}_M$  and  $\mathbf{1}_{M \times N}$  denote a  $M \times M$  identity matrix and a  $M \times N$  with all entries being 1.  $\mathcal{S}_L$  is the set of all  $L \times L$  symmetric matrices.  $\mathbf{e}_i$  is the  $i$ -th column of an identity matrix.  $\succeq$  and  $\preceq$  are used as generalized inequalities for two vectors.  $\otimes$  and  $\odot$  denote Kronecker and Hadamard product, respectively.

## II. SYSTEM MODEL

In this section, we firstly present the preliminaries of the pattern reconfigurable antenna array. Subsequently, the multipath channel model and the channel model incorporating pattern reconfigurable antenna array are introduced, respectively.

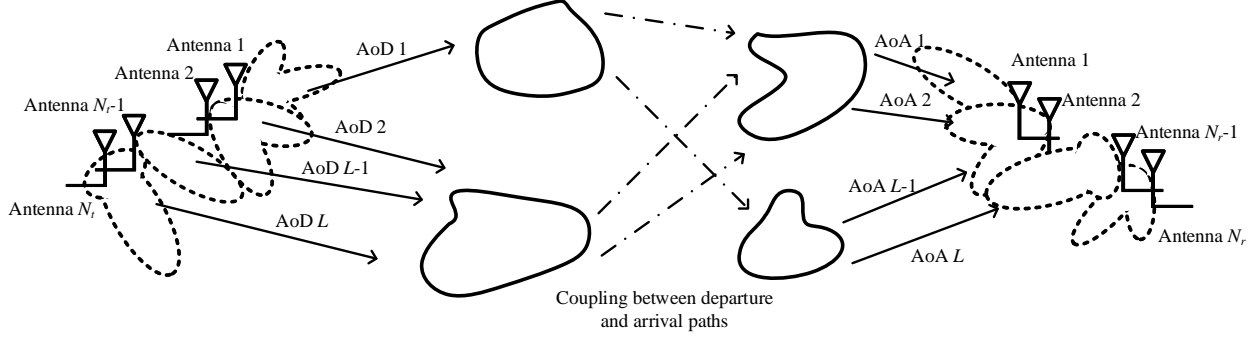


Fig. 1: Multi-path channel model for MR-MIMO.

For the pattern reconfigurable antenna array, we introduce  $\vec{f}(\theta, \phi, \mu)$  to denote the complex far-field radiation pattern, where  $\theta$  and  $\phi$  denote the corresponding vertical and horizontal angle, and  $\mu$  is the index of the antenna pattern mode. The spherical coordinate representation of the complex electric field for the  $m$ -th antenna element can be expressed as

$$\vec{f}(\theta, \phi, \mu_m) = f_\theta(\theta, \phi, \mu_m) \vec{e}_\theta + f_\phi(\theta, \phi, \mu_m) \vec{e}_\phi, \quad (1)$$

where  $\vec{e}_\theta$  and  $\vec{e}_\phi$  denote the unit vectors in the  $\theta$  and  $\phi$  direction, respectively.

#### A. Multi-Path MIMO Channel Model

We consider a single-user MIMO system in the downlink, where the number of transmit and receive antennas is  $N_t$  and  $N_r$  respectively, with  $N_r \leq N_t$ . Considering the uniform linear array (ULA) at both the BS and the receiver, the 2D physical multi-path MIMO channel model is given by [7]:

$$\mathbf{H} = \sum_{l=1}^L \alpha_l \mathbf{a}_R(\theta_l) \mathbf{a}_T^H(\varphi_l), \quad (2)$$

where  $\mathbf{H} \in \mathbb{C}^{N_r \times N_t}$  is the channel matrix with  $\mathbb{E}[\|\mathbf{H}\|_F^2] = N_t N_r$ ,  $L$  is the number of scattering paths with  $L = N_{cl} \times N_{ray}$  where  $N_{cl}$  denotes the number of scattering clusters and  $N_{ray}$  denotes the number of scattering rays in each cluster,  $\alpha_l$  is the complex gain of the  $l$ -th path. In (2),  $\mathbf{a}_R(\theta_l)$  and  $\mathbf{a}_T(\varphi_l)$  denote the receive and transmit array response vectors, where  $\theta_l$  and  $\varphi_l$  stand for the azimuth angles of arrival and departure (AoAs and AoDs), respectively. The array response vectors are given by

$$\mathbf{a}_R(\theta_l) = \frac{1}{\sqrt{N_r}} \left[ 1, e^{-j2\pi \frac{d_R}{\lambda} \sin \theta_l}, \dots, e^{-j2\pi \frac{d_R}{\lambda} (N_r-1) \sin \theta_l} \right]^T \quad (3)$$

and

$$\mathbf{a}_T(\varphi_l) = \frac{1}{\sqrt{N_t}} \left[ 1, e^{-j2\pi \frac{d_T}{\lambda} \sin \varphi_l}, \dots, e^{-j2\pi \frac{d_T}{\lambda} (N_t-1) \sin \varphi_l} \right]^T, \quad (4)$$

where  $d_T$  and  $d_R$  denote the antenna spacing at the transmitter and the receiver,  $\lambda$  is the carrier wavelength. Then (2) can be further expressed in a matrix form as:

$$\mathbf{H} = \mathbf{A}_R \mathbf{\Lambda} \mathbf{A}_T^H, \quad (5)$$

where

$$\mathbf{A}_R = [\mathbf{a}_R(\theta_1), \mathbf{a}_R(\theta_2), \dots, \mathbf{a}_R(\theta_L)] \quad (6)$$

and

$$\mathbf{A}_T = [\mathbf{a}_T(\varphi_1), \mathbf{a}_T(\varphi_2), \dots, \mathbf{a}_T(\varphi_L)] \quad (7)$$

are array response matrices of the receiver and the transmitter, and  $\mathbf{\Lambda} = \text{diag}\{\alpha_1, \alpha_2, \dots, \alpha_L\}$  is the complex channel gains of all scattering paths.

It should be noted that the above channel model  $\mathbf{H}$  only captures the physical wireless propagation environments without considering the antenna pattern at either the transmitter or the receiver. For convenience, we call it *physical channel* in the following part.

#### B. Channel Model for MR-MIMO

Fig. 1 illustrates the MR-MIMO system. Considering pattern reconfigurable antennas at both the transmitter and the receiver, the element-wise pattern reconfigurable MIMO channel model is represented as [24]

$$\tilde{\mathbf{H}}_{n,m}(\mu_m, v_n) = \sum_{l=1}^L \alpha_l \left\langle \vec{f}_T(\varphi_l, \phi_l, \mu_m), \vec{f}_R(\theta_l, \vartheta_l, v_n) \right\rangle e^{j2\pi \left( \frac{d_T}{\lambda} (m-1) \sin \varphi_l - \frac{d_R}{\lambda} (n-1) \sin \theta_l \right)}, \quad (8)$$

where  $\tilde{\mathbf{H}}_{n,m}(\mu_m, v_n)$  denotes the channel between the  $m$ -th transmit antenna with mode  $\mu_m$  and the  $n$ -th receive antenna with mode  $v_n$ , while  $\mu_m \in \mathcal{R}_m$  and  $v_n \in \mathcal{R}_n$  where  $\mathcal{R}_m$  and  $\mathcal{R}_n$  denote the continuous radiation pattern mode indication sets of the  $m$ -th transmit antenna and the  $n$ -th receive antenna,  $\vec{f}_T(\varphi_l, \phi_l, \mu_m) = [F_{v,\varphi_l,\mu_m}^{\text{Tr}}, F_{h,\phi_l,\mu_m}^{\text{Tr}}]^T$  and  $\vec{f}_R(\theta_l, \vartheta_l, v_n) = [F_{v,\theta_l,v_n}^{\text{Re}}, F_{h,\vartheta_l,v_n}^{\text{Re}}]^T$  are the electric-field (E-field) pattern vectors of corresponding antenna element with mode  $\mu_m$  at the transmitter and that with mode  $v_n$  at the receiver with AoD =  $\varphi_l$ , EoD =  $\phi_l$ , AoA =  $\theta_l$  and EoA =  $\vartheta_l$ , where EoD and EoA are abbreviations for elevation angle of departure and that of arrival, while AoD and AoA are abbreviations for azimuth angle of departure and that of arrival, respectively.  $F_v$  and  $F_h$  denote the vertical and horizontal components of the pattern vector in spherical

coordinates. Compared with (2), the effect of the antenna pattern is described by the inner product of the corresponding pattern vectors. Similarly, we term  $\tilde{\mathbf{H}}$  the *pattern channel* matrix.

The transmission process of the MR-MIMO system can be written as

$$\mathbf{y} = \tilde{\mathbf{H}}\mathbf{x} + \mathbf{n}, \quad (9)$$

where  $\mathbf{x}$  and  $\mathbf{y}$  represent transmit and receive signal vectors, and  $\mathbf{n} \sim \mathcal{CN}(0, \sigma_n^2 \mathbf{I}_{N_r})$  is the additive white Gaussian noise (AWGN) vector at the receiver side.

### C. Capacity of MR-MIMO

Assuming the perfect channel state information at the transmitter side (CSIT), the capacity for a MR-MIMO system is given by

$$C = \log_2 \det \left( \mathbf{I}_{N_r} + \frac{\rho}{N_r} \tilde{\mathbf{H}}\tilde{\mathbf{H}}^H \right), \quad (10)$$

where  $\rho$  denotes the transmit signal-to-noise ratio (SNR).

## III. CAPACITY MAXIMIZATION PATTERN DESIGN

In this section, the matrix representation of the pattern channel is proposed, based on which the capacity maximization pattern design is studied.

### A. Matrix Representation of the Pattern Channel

Firstly, we should explain the necessity of describing the pattern channel in a matrix form. At present, the pattern channel is represented in (8), which only describes the generation process of each element in the channel matrix. However, such an expression does not fully reveal how the pattern affects the channel, and meanwhile brings difficulties to the optimal pattern design.

The description in (8) can be extended to a matrix form, as shown in (11) at the bottom of this page. Based on that, the pattern channel matrix can be divided into vertical and horizontal components in spherical coordinates, which can be denoted as

$$\tilde{\mathbf{H}} = \tilde{\mathbf{H}}_v + \tilde{\mathbf{H}}_h, \quad (12)$$

where

$$\begin{aligned} \tilde{\mathbf{H}}_v &= \sum_{l=1}^L \alpha_l \mathbf{a}_R(\theta_l) \mathbf{a}_T^H(\varphi_l) \\ &\odot \left( \begin{bmatrix} F_{v,\varphi_l,\mu_1}^{\text{Tr}} F_{v,\theta_l,v_1}^{\text{Re}} & \cdots & F_{v,\varphi_l,\mu_{N_t}}^{\text{Tr}} F_{v,\theta_l,v_1}^{\text{Re}} \\ \vdots & \ddots & \vdots \\ F_{v,\varphi_l,\mu_1}^{\text{Tr}} F_{v,\theta_l,v_{N_r}}^{\text{Re}} & \cdots & F_{v,\varphi_l,\mu_{N_t}}^{\text{Tr}} F_{v,\theta_l,v_{N_r}}^{\text{Re}} \end{bmatrix} \right) \\ &= \sum_{l=1}^L \alpha_l (\mathbf{a}_R(\theta_l) \odot \mathbf{m}_{v,l}^{\text{Re}}) (\mathbf{a}_T(\varphi_l) \odot \mathbf{m}_{v,l}^{\text{Tr}})^H \\ &= (\mathbf{A}_R \odot \mathbf{M}_v^{\text{Re}}) \mathbf{\Lambda} (\mathbf{A}_T \odot \mathbf{M}_v^{\text{Tr}})^H \end{aligned} \quad (13)$$

and similarly

$$\tilde{\mathbf{H}}_h = (\mathbf{A}_R \odot \mathbf{M}_h^{\text{Re}}) \mathbf{\Lambda} (\mathbf{A}_T \odot \mathbf{M}_h^{\text{Tr}})^H. \quad (14)$$

In (13) and (14),  $\mathbf{m}_{v,l}^{\text{Tr}} = [F_{v,\varphi_l,\mu_1}^{\text{Tr}}, F_{v,\varphi_l,\mu_2}^{\text{Tr}}, \dots, F_{v,\varphi_l,\mu_{N_t}}^{\text{Tr}}]^T$  and  $\mathbf{m}_{v,l}^{\text{Re}} = [F_{v,\theta_l,v_1}^{\text{Re}}, F_{v,\theta_l,v_2}^{\text{Re}}, \dots, F_{v,\theta_l,v_{N_r}}^{\text{Re}}]^T$  are the vertical pattern sampling vectors at the transmitter and the receiver in the direction of the  $l$ -th scattering path, similarly  $\mathbf{m}_{h,l}^{\text{Tr}} = [F_{h,\varphi_l,\mu_1}^{\text{Tr}}, F_{h,\varphi_l,\mu_2}^{\text{Tr}}, \dots, F_{h,\varphi_l,\mu_{N_t}}^{\text{Tr}}]^T$  and  $\mathbf{m}_{h,l}^{\text{Re}} = [F_{h,\vartheta_l,v_1}^{\text{Re}}, F_{h,\vartheta_l,v_2}^{\text{Re}}, \dots, F_{h,\vartheta_l,v_{N_r}}^{\text{Re}}]^T$  are the horizontal ones. Combining the pattern sampling vectors together,  $\mathbf{M}_v^{\text{Tr}} = [\mathbf{m}_{v,1}^{\text{Tr}}, \mathbf{m}_{v,2}^{\text{Tr}}, \dots, \mathbf{m}_{v,L}^{\text{Tr}}]$  and  $\mathbf{M}_v^{\text{Re}} = [\mathbf{m}_{v,1}^{\text{Re}}, \mathbf{m}_{v,2}^{\text{Re}}, \dots, \mathbf{m}_{v,L}^{\text{Re}}]$  are the vertical pattern sampling matrices at the transmitter and the receiver, while  $\mathbf{M}_h^{\text{Tr}} = [\mathbf{m}_{h,1}^{\text{Tr}}, \mathbf{m}_{h,2}^{\text{Tr}}, \dots, \mathbf{m}_{h,L}^{\text{Tr}}]$  and  $\mathbf{M}_h^{\text{Re}} = [\mathbf{m}_{h,1}^{\text{Re}}, \mathbf{m}_{h,2}^{\text{Re}}, \dots, \mathbf{m}_{h,L}^{\text{Re}}]$  are the horizontal ones.

In this paper, for simplicity we consider the pattern reconfigurability at the transmitter with vertical polarization only, and in this case, the receiver pattern is simplified into

$$\begin{bmatrix} F_{v,\theta_l,v_1}^{\text{Re}} & F_{h,\vartheta_l,v_1}^{\text{Re}} \\ F_{v,\theta_l,v_2}^{\text{Re}} & F_{h,\vartheta_l,v_2}^{\text{Re}} \\ \vdots & \vdots \\ F_{v,\theta_l,v_{N_r}}^{\text{Re}} & F_{h,\vartheta_l,v_{N_r}}^{\text{Re}} \end{bmatrix} = \begin{bmatrix} 1 & 0 \\ 1 & 0 \\ \vdots & \vdots \\ 1 & 0 \end{bmatrix}, \quad (15)$$

based on which (11) is further simplified into

$$\tilde{\mathbf{H}} = \mathbf{A}_R \mathbf{\Lambda} (\mathbf{A}_T \odot \mathbf{M})^H, \quad (16)$$

where  $\mathbf{M} = \mathbf{M}_v^{\text{Tr}}$ .

From (16), it is clear that the influence of the pattern on the channel can be regarded as an additional power gain in the corresponding direction. The matrix  $\mathbf{M}$  in (16) is therefore termed as the pattern sampling matrix, whose  $(k, l)$ -th element denotes the sampling of the  $k$ -th antenna element's pattern in the direction of AoD =  $\varphi_l$ . Moreover,  $\mathbf{M}$  in (16)

$$\tilde{\mathbf{H}} = \sum_{l=1}^L \alpha_l \mathbf{a}_R(\theta_l) \mathbf{a}_T^H(\varphi_l) \odot \left( \begin{bmatrix} F_{v,\theta_l,v_1}^{\text{Re}} & F_{h,\vartheta_l,v_1}^{\text{Re}} \\ F_{v,\theta_l,v_2}^{\text{Re}} & F_{h,\vartheta_l,v_2}^{\text{Re}} \\ \vdots & \vdots \\ F_{v,\theta_l,v_{N_r}}^{\text{Re}} & F_{h,\vartheta_l,v_{N_r}}^{\text{Re}} \end{bmatrix} \begin{bmatrix} F_{v,\varphi_l,\mu_1}^{\text{Tr}} & F_{v,\varphi_l,\mu_2}^{\text{Tr}} & \cdots & F_{v,\varphi_l,\mu_{N_t}}^{\text{Tr}} \\ F_{h,\varphi_l,\mu_1}^{\text{Tr}} & F_{h,\varphi_l,\mu_2}^{\text{Tr}} & \cdots & F_{h,\varphi_l,\mu_{N_t}}^{\text{Tr}} \end{bmatrix} \right). \quad (11)$$

describes the modification process of the MIMO channel by using reconfigurable antennas, which motivates us to design the pattern, which is shown in the following.

### B. Problem Formulation

In this paper, we focus on the MR-MIMO pattern design to improve the performance over traditional MIMO. We aim to maximize the capacity of the MR-MIMO system, and the optimization problem can be expressed as  $\mathcal{P}_1$  in (17) at the bottom of this page. The first constraint enforces that the pattern should not introduce an additional power assumption, while the second one constrains  $\mathbf{M}$  to be a positive real matrix such that the pattern design only affects the power gain in the corresponding direction, without introducing additional phase adjustment overhead. Based on the properties of the Hadamard product,  $\mathcal{P}_1$  can be simplified into

$$\begin{aligned} \mathcal{P}_2 : \min_{\mathbf{X}} \quad & -\log_2 \det \left( \mathbf{I}_{N_r} + \frac{\rho}{N_r} \mathbf{A}_R \mathbf{\Lambda} (\mathbf{R}_T \odot \mathbf{X}) \mathbf{\Lambda}^H \mathbf{A}_R^H \right) \\ \text{s.t.} \quad & \text{Tr} \left( \mathbf{A}_R \mathbf{\Lambda} (\mathbf{R}_T \odot \mathbf{X}) \mathbf{\Lambda}^H \mathbf{A}_R^H \right) \leq N_r N_t, \\ & \mathbf{X} \in \mathcal{C}_L, \end{aligned} \quad (18)$$

where  $\mathbf{X} = \mathbf{M}^T \mathbf{M}$  is the real positive symmetric covariance matrix of  $\mathbf{M}$  and  $\mathcal{C}_L$  is the closed convex cone of completely positive (CP) matrices. We use  $\mathbf{X} \succeq 0$  to mean that  $\mathbf{X}$  is a positive semidefinite matrix and use  $\mathbf{X} \geq 0$  to mean that  $\mathbf{X}$  is entry-wise nonnegative.

Define the sets of CP matrices and doubly nonnegative (DNN) matrices as below [30]

$$\begin{aligned} \mathcal{C}_L &:= \{ \mathbf{X} \in \mathcal{S}_L : \mathbf{X} = \mathbf{N} \mathbf{N}^T \text{ for some } \mathbf{N} \geq 0 \}, \\ \mathcal{D}_L &:= \{ \mathbf{X} \in \mathcal{S}_L : \mathbf{X} \succeq 0, \mathbf{X} \geq 0 \}. \end{aligned} \quad (19)$$

It is obvious that each CP matrix is DNN, i.e.,  $\mathcal{C}_L \subseteq \mathcal{D}_L$ , but the reverse is generally not true. Therefore,  $\mathcal{P}_2$  can be

relaxed as

$$\begin{aligned} \mathcal{P}_3 : \min_{\mathbf{X}} \quad & -\log_2 \det \left( \mathbf{I}_{N_r} + \frac{\rho}{N_r} \mathbf{A}_R \mathbf{\Lambda} (\mathbf{R}_T \odot \mathbf{X}) \mathbf{\Lambda}^H \mathbf{A}_R^H \right) \\ \text{s.t.} \quad & \text{Tr} \left( \mathbf{A}_R \mathbf{\Lambda} (\mathbf{R}_T \odot \mathbf{X}) \mathbf{\Lambda}^H \mathbf{A}_R^H \right) \leq N_r N_t, \\ & \mathbf{X} \in \mathcal{D}_L. \end{aligned} \quad (20)$$

The equivalence between  $\mathcal{P}_2$  and  $\mathcal{P}_3$  is conditional. Firstly, it is shown in [30] that  $L \leq 4$ ,  $\mathcal{C}_L = \mathcal{D}_L$ . Secondly, a DNN matrix  $\mathbf{X}$  is also a CP matrix when  $\text{rank}(\mathbf{X}) = 1$ , which reveals that the equivalence between  $\mathcal{P}_2$  and  $\mathcal{P}_3$  holds in the single-pattern case, which will be discussed in Section IV.

We have the following proposition to discuss the convexity of  $\mathcal{P}_3$ .

*Proposition 1:* The cost function of  $\mathcal{P}_3$  is convex and thus problem  $\mathcal{P}_3$  is convex [31].

Despite the convexity, the Hadamard product is not easy to handle. Therefore, we further transform the cost function of  $\mathcal{P}_3$ , as shown in (21) at the bottom of this page, where  $\tilde{\mathbf{A}}_R = \mathbf{A}_R \mathbf{\Lambda} = [\tilde{\mathbf{a}}_{R,1}, \tilde{\mathbf{a}}_{R,2}, \dots, \tilde{\mathbf{a}}_{R,L}]$  is the composite receiver array response matrix which describes the power gain and the directivity of the scattering path simultaneously.  $\mathbf{a}_i = \alpha_i \mathbf{a}_{R,i} \mathbf{a}_{T,i}^H$  denotes the composite subchannel matrix of the  $i$ -th scattering path. With  $\mathbf{A}_{N_t L \times N_r} = [\mathbf{A}_1^*, \mathbf{A}_2^*, \dots, \mathbf{A}_L^*]^T$ ,  $\mathcal{P}_3$  can be further simplified into  $\mathcal{P}_4$  as

$$\begin{aligned} \mathcal{P}_4 : \min_{\mathbf{X}} \quad & -\log_2 \det \left( \mathbf{I}_{N_r} + \frac{\rho}{N_r} \mathbf{A}^H (\mathbf{X} \otimes \mathbf{I}_{N_t}) \mathbf{A} \right) \\ \text{s.t.} \quad & \text{Tr} \left( \mathbf{A}^H (\mathbf{X} \otimes \mathbf{I}_{N_t}) \mathbf{A} \right) \leq N_r N_t, \\ & \mathbf{X}_{i,j} \geq 0, \mathbf{X} = \mathbf{X}^T, \mathbf{X} \succeq 0. \end{aligned} \quad (22)$$

$\mathcal{P}_4$  is equivalent to  $\mathcal{P}_3$ , which is a convex semidefinite programming (SDP) problem and can be solved by CVX directly. Although  $\mathcal{P}_2$  can be solved via solving  $\mathcal{P}_4$  using the semidefinite relaxation (SDR) when  $\text{rank}(\mathbf{X}) = 1$ , a more efficient solution for the single-pattern case is needed. What's more, the study of pattern design for the multi-pattern case is still blank. In what follows, we will propose the pattern

---


$$\begin{aligned} \mathcal{P}_1 : \max_{\mathbf{M}} \quad & \log_2 \det \left( \mathbf{I}_{N_r} + \frac{\rho}{N_r} \mathbf{A}_R \mathbf{\Lambda} (\mathbf{A}_T \odot \mathbf{M})^H (\mathbf{A}_T \odot \mathbf{M}) \mathbf{\Lambda}^H \mathbf{A}_R^H \right) \\ \text{s.t.} \quad & \text{Tr} \left( \mathbf{A}_R \mathbf{\Lambda} (\mathbf{A}_T \odot \mathbf{M})^H (\mathbf{A}_T \odot \mathbf{M}) \mathbf{\Lambda}^H \mathbf{A}_R^H \right) \leq N_r N_t, \\ & \mathbf{M}_{i,j} \geq 0 \quad i, j = 1, 2, \dots, L. \end{aligned} \quad (17)$$


---

$$\begin{aligned} & -\log_2 \det \left( \mathbf{I}_{N_r} + \frac{\rho}{N_r} \mathbf{A}_R \mathbf{\Lambda} (\mathbf{R}_T \odot \mathbf{X}) \mathbf{\Lambda}^H \mathbf{A}_R^H \right) \\ & = -\log_2 \det \left( \mathbf{I}_{N_r} + \frac{\rho}{N_r} [\tilde{\mathbf{a}}_{R,1}, \dots, \tilde{\mathbf{a}}_{R,L}] \begin{bmatrix} x_{1,1} \mathbf{a}_{T,1}^H \mathbf{a}_{T,1} & \cdots & x_{1,L} \mathbf{a}_{T,1}^H \mathbf{a}_{T,L} \\ \vdots & \ddots & \vdots \\ x_{L,1} \mathbf{a}_{T,L}^H \mathbf{a}_{T,1} & \cdots & x_{L,L} \mathbf{a}_{T,L}^H \mathbf{a}_{T,L} \end{bmatrix} \begin{bmatrix} \tilde{\mathbf{a}}_{R,1}^H \\ \vdots \\ \tilde{\mathbf{a}}_{R,L}^H \end{bmatrix} \right), \\ & = -\log_2 \det \left( \mathbf{I}_{N_r} + \frac{\rho}{N_r} [\mathbf{A}_1, \dots, \mathbf{A}_L] \begin{bmatrix} x_{1,1} \mathbf{I}_{N_t} & \cdots & x_{1,L} \mathbf{I}_{N_t} \\ \vdots & \ddots & \vdots \\ x_{L,1} \mathbf{I}_{N_t} & \cdots & x_{L,L} \mathbf{I}_{N_t} \end{bmatrix} \begin{bmatrix} \mathbf{A}_1^H \\ \vdots \\ \mathbf{A}_L^H \end{bmatrix} \right). \end{aligned} \quad (21)$$

designing algorithms for both the single-pattern and multi-pattern cases.

*Insight:* The form of  $\mathcal{P}_4$  reveals that the influence of the pattern on capacity is applied through the covariance matrix of the pattern sampling matrix. In other words, if different patterns lead to the same covariance matrix, they will achieve the same capacity. This is a great advantage in practical pattern design, because we can choose the pattern with the lowest physical implementation cost after obtaining the optimal pattern covariance matrix.

#### IV. PROPOSED PATTERN DESIGN ALGORITHM

The CP constraint of  $\mathcal{P}_2$  brings difficulties to the solution of the optimization problem. Although the equivalence between  $\mathcal{P}_2$  and  $\mathcal{P}_4$  when  $\text{rank}(\mathbf{X}) = 1$  makes it possible to solve  $\mathcal{P}_2$  via solving  $\mathcal{P}_4$  using the SDR algorithm, the rank-1 solution cannot be guaranteed and the principle of the pattern design problem cannot be revealed. Thus, an efficient pattern design algorithm is needed. Therefore in this section, we consider alternative solutions to the pattern design problem. In particular, we firstly study a simplified case where all the antennas adopt the same radiation pattern, and then extend to a more generic case where each antenna can adopt different radiation patterns.

##### A. Single-Pattern Case

When each antenna element employs the same radiation pattern, mathematically it is equivalent to that all the entries in each column of  $\mathbf{M}$  have the same value, which makes  $\mathbf{M}$  a rank-one matrix. With  $\mathbf{M} = \mathbf{1}_{N_t \times 1} \mathbf{m}^T$  where  $\mathbf{m} = [m_1, m_2, \dots, m_L]^T$ , (16) can be further simplified as

$$\begin{aligned} \tilde{\mathbf{H}} &= \mathbf{A}_R \mathbf{\Lambda} (\mathbf{A}_T \odot \mathbf{M})^H \\ &= \mathbf{A}_R \mathbf{\Lambda} (\mathbf{A}_T \text{diag}\{[m_1, m_2, \dots, m_L]\})^H \\ &= \sum_{i=1}^L \tilde{\alpha}_i \mathbf{H}_i, \end{aligned} \quad (23)$$

where  $\mathbf{H}_i = \mathbf{a}_{R,i} \mathbf{a}_{T,i}^H$  denotes the  $i$ -th subchannel matrix, and  $\tilde{\alpha}_i = \alpha_i m_i$  denotes the redistributed channel gain of the  $i$ -th scattering path which reveals the effect of the pattern. (23) reveals that the effect of the pattern design is equivalent to the redistribution of power to all scattering paths.

From the perspective of the singular value optimization, (10) can be transformed into

$$\begin{aligned} & -\log_2 \det \left( \mathbf{I}_{N_r} + \frac{\rho}{N_r} \tilde{\mathbf{H}} \tilde{\mathbf{H}}^H \right) \\ &= -\log_2 \prod_{i=1}^r \left( 1 + \frac{\rho}{N_r} |\sigma_i(\tilde{\mathbf{H}})|^2 \right), \end{aligned} \quad (24)$$

where  $r = \text{rank}(\tilde{\mathbf{H}})$  and  $\sigma_i(\tilde{\mathbf{H}})$  denote the rank of  $\tilde{\mathbf{H}}$  and the  $i$ -th singular value of  $\tilde{\mathbf{H}}$ , respectively. Based on (23) and

(24), the pattern design problem in the single-pattern case can be generalized into:

$$\begin{aligned} \mathcal{P}_5 : \min_{\{x_i\}} & -\prod_{i=1}^r (1 + \gamma x_i) \\ \text{s.t.} & \sum_{i=1}^r x_i - N_r N_t \leq 0, \\ & \gamma = \frac{\rho}{N_r}, \end{aligned} \quad (25)$$

where

$$x_i = \left| \sigma_i(\tilde{\mathbf{H}}) \right|^2 = \left| \sigma_i \left( \sum_{l=1}^L \tilde{\alpha}_l \mathbf{H}_l \right) \right|^2. \quad (26)$$

Without considering (26), the optimal solution  $\{x_i^*\}$  of  $\mathcal{P}_5$  can be obtained easily through the Karush-Kuhn-Tucker (KKT) conditions. However, the non-convexity introduced by (26) generally excludes  $\{x_i^*\}$  from the feasible region.

(25) and (26) exhibit a clear physical interpretation that the capacity of the channel is equivalent to the sum capacity of the independent eigen-subchannels. Each eigenvalue is the quantitative description of how much communication resource can be distributed to the corresponding eigen-subchannel. Similar to the principle of water-filling, a "good" channel means that the singular values of the channel matrix are distributed as even as possible, and vice versa. Based on that, we propose an eigenvalue optimization based power allocation scheme that aims to balance the singular values of  $\tilde{\mathbf{H}}$ , i.e., minimizing the maximum singular value of  $\tilde{\mathbf{H}}$ , given by

$$\begin{aligned} \mathcal{P}_6 : \min_{\mathbf{p}} & \sigma_{\max}(\tilde{\mathbf{H}}) = \sigma_{\max} \left( \sum_{l=1}^L p_l \mathbf{H}_l \right) \\ \text{s.t.} & \sum_{l=1}^L p_l = 1, p_l \geq 0, \end{aligned} \quad (27)$$

where  $\mathbf{p} = [p_1, p_2, \dots, p_L]^T$  is the power allocation vector.  $\mathcal{P}_6$  can be transformed into

$$\begin{aligned} \mathcal{P}_7 : \min_{\mathbf{p}} & \lambda_{\max}(\tilde{\mathbf{W}}) = \lambda_{\max} \left( \sum_{l=1}^L p_l \mathbf{W}_l \right) \\ \text{s.t.} & \sum_{l=1}^L p_l = 1, p_l \geq 0, \end{aligned} \quad (28)$$

where  $\tilde{\mathbf{W}} = [\mathbf{0}, \tilde{\mathbf{H}}; \tilde{\mathbf{H}}^H, \mathbf{0}]$  and  $\mathbf{W}_l = [\mathbf{0}, \mathbf{H}_l; \mathbf{H}_l^H, \mathbf{0}]$  so that  $\lambda_{\max}(\tilde{\mathbf{W}}) = \sigma_{\max}(\tilde{\mathbf{H}})$  and  $\lambda_{\max}(\mathbf{W}_l) = \sigma_{\max}(\mathbf{H}_l)$ .  $\lambda_{\max}(\tilde{\mathbf{W}})$  is the maximum eigenvalue of matrix  $\tilde{\mathbf{W}}$ .  $\mathcal{P}_7$  can be further simplified as a SDP problem:

$$\begin{aligned} \mathcal{P}_8 : \min_{\mathbf{p}, t} & t \\ \text{s.t.} & \sum_{l=1}^L p_l \mathbf{W}_l - t \mathbf{I}_{N_t + N_r} \preceq \mathbf{0}, \\ & \sum_{l=1}^L p_l = 1, p_l \geq 0. \end{aligned} \quad (29)$$

$\mathcal{P}_8$  can be solved via CVX directly by expanding the first constraint into its equivalent real and imaginary representations. We introduce the power scaling factor  $\delta$ , given by (30) to ensure the satisfaction of the power constraint to the pattern channel matrix.

$$\begin{aligned} & \left\| \delta \sum_{l=1}^L p_l \mathbf{H}_l \right\|_{\text{F}}^2 = N_t N_r \\ \Leftrightarrow & \delta^2 \text{Tr} \left( \left( \sum_{l=1}^L p_l \mathbf{H}_l \right)^{\text{H}} \left( \sum_{l=1}^L p_l \mathbf{H}_l \right) \right) = N_t N_r, \quad (30) \\ \Leftrightarrow & \delta = \sqrt{\frac{N_t N_r}{\text{Tr} \left( \left( \sum_{l=1}^L p_l \mathbf{H}_l \right)^{\text{H}} \left( \sum_{l=1}^L p_l \mathbf{H}_l \right) \right)}}. \end{aligned}$$

Let  $|\tilde{\alpha}_l| = p_l \delta$  for all  $l = 1, 2, \dots, L$ . Then the corresponding  $m_l$  of each scattering path is given by

$$m_l = \frac{|\tilde{\alpha}_l|}{|\alpha_l|} = \frac{p_l \delta}{|\alpha_l|}. \quad (31)$$

### B. Multi-Pattern Case

When each antenna element employs a different pattern, (16) can be transformed into

$$\begin{aligned} \tilde{\mathbf{H}} &= \mathbf{A}_R \mathbf{\Lambda} (\mathbf{A}_T \odot \mathbf{M})^{\text{H}} \\ &= \sum_{i=1}^L \alpha_i \mathbf{a}_{R,i} (\mathbf{a}_{T,i} \odot \mathbf{M}(:, i))^{\text{H}} \\ &= \sum_{i=1}^L \alpha_i p_i \mathbf{a}_{R,i} (\mathbf{a}_{T,i} \odot \widehat{\mathbf{m}}_i)^{\text{H}} = \sum_{i=1}^L \alpha_i p_i \widehat{\mathbf{H}}_i, \end{aligned} \quad (32)$$

where  $\widehat{\mathbf{H}}_i = \mathbf{a}_{R,i} (\mathbf{a}_{T,i} \odot \widehat{\mathbf{m}}_i)^{\text{H}}$  is the  $i$ -th normalized modified subchannel with  $\left\| \widehat{\mathbf{H}}_i \right\|_{\text{F}}^2 = 1$  and  $p_i$  is the power we distribute to the corresponding subchannel.  $\widehat{\mathbf{m}}_i = \frac{1}{p_i} \mathbf{M}(:, i)$  with  $\|\widehat{\mathbf{m}}_i\|_2^2 = N_t$  denotes the correlation modification vector of the  $i$ -th scattering path.

*Proposition 2:* The constraint  $\|\widehat{\mathbf{m}}_i\|_2^2 = N_t$  is equivalent to  $\left\| \widehat{\mathbf{H}}_i \right\|_{\text{F}}^2 = 1$ .

*Proof:* See Appendix.

From (32), we can observe the superiority of the multi-pattern case on the wireless channel for MR-MIMO systems over the single-pattern case in Section IV-A. Compared with (23), the introduction of  $\widehat{\mathbf{m}}_i$  offers the ability to modify the subchannel matrix, which will change the correlation among each subchannel. Based on that, the system can redistribute power with a better correlation structure.

In order to quantify the correlation structure of the pattern channel, we first present the covariance matrix  $\widehat{\mathbf{G}} \in \mathbb{C}^{L \times L}$  of subchannels as (33) at the bottom of this page. The  $(i, j)$ -th element of  $\widehat{\mathbf{G}}$  describes the correlation of  $\widehat{\mathbf{H}}_i$  and  $\widehat{\mathbf{H}}_j$ , and it is obvious that  $\widehat{\mathbf{G}}$  is a Hermitian matrix. Based on  $\widehat{\mathbf{G}}$ , we define a correlation level indication vector in the following form:

$$\hat{\mathbf{g}} = \left[ \sum_{j=2}^L \left| \widehat{\mathbf{G}}_{1,j} \right|^2, \sum_{j=1, j \neq 2}^L \left| \widehat{\mathbf{G}}_{2,j} \right|^2, \dots, \sum_{j=1}^{L-1} \left| \widehat{\mathbf{G}}_{L,j} \right|^2 \right]^{\text{T}}, \quad (34)$$

which quantifies the sum correlation effect of each subchannel with all the other subchannels.

Based on the above analysis, the efficient pattern design for the multi-pattern case can be decomposed into two steps. Firstly, we design the correlation modification matrix  $\widehat{\mathbf{M}} = [\widehat{\mathbf{m}}_1, \widehat{\mathbf{m}}_2, \dots, \widehat{\mathbf{m}}_L]$  to optimize the correlation structure of the pattern channel. Subsequently, based on the optimized correlation structure, we adopt the power allocation scheme introduced in Section IV-A to further improve the channel quality. In the following, we study the correlation modification problem.

Recall that the correlation coefficient between the  $i$ -th subchannel  $\widehat{\mathbf{H}}_i$  and the  $j$ -th subchannel  $\widehat{\mathbf{H}}_j$  is given by (33) at the bottom of this page. We can observe that the design of a single  $\widehat{\mathbf{m}}_i$  will have an impact on the related  $(L-1)$  correlation coefficients, which brings difficulties to decouple the design of each  $\widehat{\mathbf{m}}_i$ .

To deal with this problem, we adopt a sequential optimization framework, which sequentially updates the  $L$  correlation modification vectors in an adaptive manner. The physical principle of the sequential optimization framework is to optimize the selected correlation vector in each iteration, so that the modified subchannel can maintain low correlation with all of the previously modified subchannels. For each correlation modification vector, we formulate the optimization problem and present the algorithm based on manifold optimization and eigenvalue decomposition, as described below.

1) *Subproblem in SOF:* To begin with, the correlation modification matrix  $\widehat{\mathbf{M}}$  is initialized as  $\mathbf{1}_{M \times N}$ , which means that there is no correlation modification for all subchannels. In the  $i$ -th iteration, we calculate the covariance matrix of each subchannel to obtain the correlation indication vector  $\hat{\mathbf{g}}$  in (34). After sorting the entries of  $\hat{\mathbf{g}}$  in a descending order, we can obtain the subchannel with the largest correlation level that is to be updated within the current iteration, whose index is denoted by  $n_i$ . Without loss of generality, considering the correlation coefficient between the  $n_k$ -th and the  $n_i$ -th

$$\begin{aligned} \widehat{\mathbf{G}}_{i,j} &= \text{Tr} \left( \widehat{\mathbf{H}}_i^{\text{H}} \widehat{\mathbf{H}}_j \right) \\ &= \text{Tr} \left( (\mathbf{a}_{T,i} \odot \widehat{\mathbf{m}}_i)^{\text{H}} \mathbf{a}_{R,i}^{\text{H}} \mathbf{a}_{R,j} (\mathbf{a}_{T,j} \odot \widehat{\mathbf{m}}_j)^{\text{H}} \right) \\ &= \frac{1}{N_r N_t} \sum_{n=1}^{N_r} e^{j2\pi \frac{d_{\text{R}}}{\lambda} (n-1)(\sin \theta_j - \sin \theta_i)} \sum_{k=1}^{N_t} \widehat{\mathbf{m}}_i(k) \widehat{\mathbf{m}}_j(k) e^{j2\pi \frac{d_{\text{T}}}{\lambda} (k-1)(\sin \varphi_i - \sin \varphi_j)}. \end{aligned} \quad (33)$$

normalized channel with  $k \leq i-1$ , (33) can be simplified as

$$\widehat{\mathbf{G}}_{n_i, n_k} = \rho_{n_i, n_k}^R \mathbf{b}_{n_i, n_k}^T \widehat{\mathbf{m}}_{n_i}, \quad (35)$$

where

$$\mathbf{b}_{n_i, n_k}(n) = \frac{1}{N_t} \widehat{\mathbf{m}}_{n_k}(n) e^{j2\pi \frac{d_T}{\lambda} (n-1) (\sin \varphi_{n_i} - \sin \varphi_{n_k})} \quad (36)$$

and  $\rho_{n_i, n_k}^R = \frac{1}{N_r} \sum_{n=1}^{N_r} e^{j2\pi \frac{d_R}{\lambda} (n-1) (\sin \theta_{n_k} - \sin \theta_{n_i})}$  denotes the correlation coefficient between the receive array response vectors of the corresponding subchannels. To minimize the correlation coefficient between the  $n_k$ -th modified subchannel and the  $n_i$ -th updated subchannel, we consider the following optimization problem:

$$\begin{aligned} \mathcal{P}_9 : \min_{\widehat{\mathbf{m}}_{n_i}} & \left| \widehat{\mathbf{G}}_{n_i, n_k} \right|^2 \\ \text{s.t.} & \widehat{\mathbf{m}}_{n_i}^T \widehat{\mathbf{m}}_{n_i} = N_t, \\ & \widehat{\mathbf{m}}_{n_i} \geq 0, \end{aligned} \quad (37)$$

where

$$\begin{aligned} \left| \widehat{\mathbf{G}}_{n_i, n_k} \right|^2 &= \left| \rho_{n_i, n_k}^R \right|^2 \left( \mathbf{b}_{n_i, n_k}^T \widehat{\mathbf{m}}_{n_i} \right)^H \mathbf{b}_{n_i, n_k}^T \widehat{\mathbf{m}}_{n_i} \\ &= \left| \rho_{n_i, n_k}^R \right|^2 \widehat{\mathbf{m}}_{n_i}^T \left( \mathbf{b}_{n_i, n_k}^* \mathbf{b}_{n_i, n_k}^T \right) \widehat{\mathbf{m}}_{n_i} \\ &= \widehat{\mathbf{m}}_{n_i}^T \text{real} \left\{ \left| \rho_{n_i, n_k}^R \right|^2 \mathbf{b}_{n_i, n_k}^* \mathbf{b}_{n_i, n_k}^T \right\} \widehat{\mathbf{m}}_{n_i} \\ &= \widehat{\mathbf{m}}_{n_i}^T \mathbf{B}_{n_k} \widehat{\mathbf{m}}_{n_i} \end{aligned} \quad (38)$$

and the first constraint is the power constraint that ensures  $\left\| \widehat{\mathbf{H}}_{n_i} \right\|_F^2 = 1$ . Considering that the real quadratic form will not be influenced by the imaginary component of the conjugate symmetric coefficient matrix, the cost function of  $\mathcal{P}_9$  can be simplified by defining  $\mathbf{B}_{n_k} = \text{real} \left\{ \left| \rho_{n_i, n_k}^R \right|^2 \mathbf{b}_{n_i, n_k}^* \mathbf{b}_{n_i, n_k}^T \right\}$ .

Considering all the  $(i-1)$  previously updated subchannels, the optimization problem in the  $i$ -th iteration is constructed as follows:

$$\begin{aligned} \mathcal{P}_{10} : \min_{\widehat{\mathbf{m}}_{n_i}} & \widehat{\mathbf{m}}_{n_i}^T \left( \sum_{k=1}^{i-1} \mathbf{B}_{n_k} \right) \widehat{\mathbf{m}}_{n_i} \\ \text{s.t.} & \widehat{\mathbf{m}}_{n_i}^T \widehat{\mathbf{m}}_{n_i} = N_t, \\ & \widehat{\mathbf{m}}_{n_i} \geq 0. \end{aligned} \quad (39)$$

2) *Manifold Optimization based Algorithm for Solving (39):*  $\mathcal{P}_{10}$  is non-convex because of the quadratic equality constraint. Nevertheless,  $\mathcal{P}_{10}$  can readily be solved using the conjugate gradient algorithm based on manifold optimization [32]. The basic idea of manifold optimization is to handle the nonconvex problem in a Riemannian manifold space, and some optimization algorithms such as the conjugate gradient descend method can be analogously extended to the manifold space.

Defining the real circle as  $\mathcal{M} = \{ \mathbf{x} \in \mathbb{R}^m : \mathbf{x}^T \mathbf{x} = 1 \}$ , the gradient vector of the cost function at a given point  $\mathbf{x} \in \mathcal{M}$  can be projected onto the tangent space  $T_{\mathbf{x}} \mathcal{M}$

$$\begin{aligned} \text{grad } f(\mathbf{x}) &= \text{Proj}_{\mathbf{x}} \nabla f(\mathbf{x}) \\ &= \nabla f(\mathbf{x}) - \nabla f(\mathbf{x}) \odot \mathbf{x}^2, \end{aligned} \quad (40)$$

where  $\nabla f(\mathbf{x})$  is the Euclidean gradient of the cost function. It can be verified that the Euclidean and Riemannian gradients of the objective function in (39) are

$$\nabla f(\mathbf{x}) = 2 \left( \sum_{k=1}^{i-1} \mathbf{B}_{n_k} \right) \mathbf{x} \quad (41)$$

and

$$\text{grad } f(\mathbf{x}) = 2 \left( \sum_{k=1}^{i-1} \mathbf{B}_{n_k} \right) \mathbf{x} \odot (\mathbf{1} - \mathbf{x}^2). \quad (42)$$

After determining the decent step using Armijo backtracking line search, we retract the descend vector to the manifold using the following operator

$$\begin{aligned} \text{Retr}_{\mathbf{x}} : T_{\mathbf{x}} \mathcal{M} &\rightarrow \mathcal{M} : \\ \alpha \mathbf{d} &\mapsto \text{Retr}_{\mathbf{x}}(\alpha \mathbf{d}) = \text{vec} \left[ \frac{(\mathbf{x} + \alpha \mathbf{d})_i}{\|(\mathbf{x} + \alpha \mathbf{d})_i\|} \right], \end{aligned} \quad (43)$$

where  $\alpha$  denotes the step size and  $\mathbf{d}$  denotes the descent direction in the tangent space. The overall algorithm is summarized in Algorithm 1, and the convergence of the algorithm can be guaranteed according to Theorem 4.3.1 in [32], [33].

---

**Algorithm 1** Conjugate Gradient Algorithm Based on Manifold Optimization for Solving  $\mathcal{P}_{10}$

---

**Input:**  $\mathbf{B} = \sum_{k=1}^{i-1} \mathbf{B}_{n_k}$ ,  $\epsilon$ ,  $T_{max}$

**Output:**  $\widehat{\mathbf{m}}_{n_i}$

- 1: Initialize  $\mathbf{m}^{(0)}$  as  $\mathbf{1}_{N_i \times 1}$  and set  $k = 1$ ;
  - 2: Calculate  $\text{grad } f(\mathbf{m}^{(0)})$  via (42) and obtain  $\mathbf{d}^{(0)} = -\text{grad } f(\mathbf{m}^{(0)})$ ;
  - 3: **for**  $|f(\mathbf{m}^{(k)}) - f(\mathbf{m}^{(k-1)})| \geq \epsilon$  and  $k \leq T_{max}$  **do**
  - 4:   Choose Armijo backtracking line search step size  $\alpha^{(k)}$ ;
  - 5:   Find the updated  $\mathbf{m}^{(k+1)}$  via (43):  $\mathbf{m}^{(k+1)} = \text{Retr}_{\mathbf{m}^{(k)}}(\alpha^{(k)} \mathbf{d}^{(k)})$ ;
  - 6:   Calculate gradient vector:  $\mathbf{g}^{(k+1)} = \text{grad } f(\mathbf{m}^{(k+1)})$  via (40)-(42);
  - 7:   Choose Polak-Ribiere parameter  $\beta^{(k+1)} = \frac{\text{grad } f^T(\mathbf{m}^{(k+1)})(\text{grad } f(\mathbf{m}^{(k+1)}) - \text{grad } f(\mathbf{m}^{(k)}))}{\|\text{grad } f(\mathbf{m}^{(k)})\|_2^2}$ ;
  - 8:   Calculate conjugate direction  $\mathbf{d}^{(k+1)} = -\mathbf{g}^{(k+1)} + \beta^{(k+1)} \mathbf{d}^{(k)}$ ;
  - 9:    $k = k + 1$ ;
  - 10: **end for**
  - 11: Calculate the power scaling factor  $\tau = \sqrt{\frac{N_i}{\|\max\{\mathbf{m}^{(k)}, \mathbf{0}\}\|_2^2}}$  and obtain  $\widehat{\mathbf{m}}_{n_i}^* = \tau \max\{\mathbf{m}^{(k)}, \mathbf{0}\}$ ;
- 

3) *Eigenvalue Decomposition based Algorithm for Solving (39):* Considering that the linear search process in the above Algorithm 1 might be computationally expensive, we propose a low-complexity alternative approach. To be more specific, based on the eigenvalue decomposition of  $\mathbf{B} = \sum_{k=1}^{i-1} \mathbf{B}_{n_k} = \mathbf{U} \mathbf{\Sigma} \mathbf{U}^T$ ,  $\mathcal{P}_{10}$  can be simplified as

$$\begin{aligned} \mathcal{P}_{11} : \min_{\mathbf{m}} & (\mathbf{U}^T \mathbf{m})^T \mathbf{\Sigma} (\mathbf{U}^T \mathbf{m}) \\ \text{s.t.} & \mathbf{m}^T \mathbf{m} = N_t, \\ & \mathbf{m} \geq 0, \end{aligned} \quad (44)$$



where  $\mathbf{U}$  is an  $N_t \times N_t$  real orthogonal matrix and  $\mathbf{\Sigma}$  is the diagonal eigenvalue matrix. With  $\mathbf{w} = \mathbf{U}^T \mathbf{m}$ ,  $\mathcal{P}_{11}$  can be transformed into  $\mathcal{P}_{12}$ :

$$\begin{aligned} \mathcal{P}_{12} : \min_{\mathbf{w}} \quad & \mathbf{w}^T \mathbf{\Sigma} \mathbf{w} \\ \text{s.t.} \quad & \mathbf{w}^T \mathbf{w} = N_t, \\ & \mathbf{U} \mathbf{w} \geq 0. \end{aligned} \quad (45)$$

Let  $\mathbf{w}^* = \sqrt{N_t} \mathbf{e}_{\min}$  where  $\mathbf{e}_{\min}$  denotes a unit vector whose non-zero entry corresponds to the location of the smallest eigenvalue of  $\mathbf{B}$  in  $\text{diag}\{\mathbf{\Lambda}\}$  [34]. Therefore, a feasible solution to  $\mathcal{P}_{11}$  can thus be obtained by

$$\widehat{\mathbf{m}}_{n_i}^* = \kappa \max\{\mathbf{U} \mathbf{w}^*, \mathbf{0}\}, \quad (46)$$

where  $\kappa = \sqrt{\frac{N_t}{\|\max\{\mathbf{U} \mathbf{w}^*, \mathbf{0}\}\|_2^2}}$  is the power scaling factor to ensure the satisfaction of  $\|\widehat{\mathbf{m}}_{n_i}^*\|_2^2 = N_t$ .

Considering the non-convexity introduced by the quadratic equality constraint, it is difficult to obtain the optimal solution of  $\mathcal{P}_{10}$ . Fortunately, the mechanism of the SOF returns a point with a promising performance of the correlation modification process. The overall algorithm for the sequential optimization framework is summarized in Algorithm 2.

---

#### Algorithm 2 Sequential Optimization Framework (SOF)

---

**Input:**  $\mathbf{A}_R, \mathbf{A}_T, \mathbf{\Lambda}$

**Output:**  $\mathbf{M}$

- 1: Initialize  $\mathcal{I} = \emptyset$  and  $\widehat{\mathbf{M}} = \mathbf{1}_{N_t \times L}$ ;
  - 2: Calculate  $\mathbf{H}_i = \mathbf{a}_{R,i} \mathbf{a}_{T,i}^H$ ; Obtain  $\mathcal{S} = \{\mathbf{H}_i \mid i = 1, 2, \dots, L\}$ ;
  - 3: Calculate  $\widehat{\mathbf{G}}^{(1)}$  based on (33); Calculate  $\widehat{\mathbf{g}}^{(1)}$  based on (34);
  - 4: Find  $n_1$  such that  $\widehat{\mathbf{g}}_{n_1}^{(1)} = \max\{\widehat{\mathbf{g}}^{(1)}\}$ ; Stack  $\mathcal{I} = [\mathcal{I}, n_1]$ ;
  - 5: **for**  $i = 2 : L$  **do**
  - 6:   Remove  $\widehat{\mathbf{g}}_j^{(i-1)}$  from  $\widehat{\mathbf{g}}^{(i-1)}$  and obtain  $\widehat{\mathbf{g}}', \forall j \in \mathcal{I}$ ;
  - 7:   Find  $n_i$  such that  $\widehat{\mathbf{g}}_{n_i}^{(i)} = \max\{\widehat{\mathbf{g}}'\}$ ; Stack  $\mathcal{I} = [\mathcal{I}, n_i]$ ;
  - 8:   Initialize  $\mathbf{B}_i = \mathbf{0}_{L \times L}$ ;
  - 9:   **for**  $k = 1 : (i - 1)$  **do**
  - 10:     Obtain  $n_k = \mathcal{I}(k)$ ;
  - 11:     Calculate  $\mathbf{b}_{n_i, n_k}$  based on (36);
  - 12:     Obtain  $\mathbf{B}_{n_k} = \mathbf{b}_{n_i, n_k}^* \mathbf{b}_{n_i, n_k}^T$ ;
  - 13:     Update  $\mathbf{B}_i = \mathbf{B}_i + \mathbf{B}_{n_k}$ ;
  - 14:   **end for**
  - 15:   Solve  $\mathcal{P}_{10}$  and obtain  $\widehat{\mathbf{m}}_{n_i}^*$ ;
  - 16:   Update  $\widehat{\mathbf{M}}(:, n_i) = \widehat{\mathbf{m}}_{n_i}^*$ ;
  - 17:   Update  $\widehat{\mathbf{H}}_{n_i} = \mathbf{a}_{R, n_i} \left( \mathbf{a}_{T, n_i} \odot \widehat{\mathbf{M}}(:, n_i) \right)^H$ ;
  - 18:   Calculate  $\widehat{\mathbf{G}}^{(i)}$  based on (33); Calculate  $\widehat{\mathbf{g}}^{(i)}$  based on (34);
  - 19: **end for**
  - 20: Obtain  $\widehat{\mathcal{S}} = \{\widehat{\mathbf{H}}_i \mid i = 1, 2, \dots, L\}$ ;
  - 21: Calculate  $\widehat{\mathbf{G}}$  based on (33); Calculate  $\widehat{\mathbf{g}}$  based on (34);
  - 22: Solve  $\mathcal{P}_8$  and obtain  $\mathbf{p}$ ;
  - 23: Obtain  $m_i$  based on (31);
  - 24: Output  $\mathbf{M} = \widehat{\mathbf{M}} \text{diag}\{m_i\}$ ;
- 

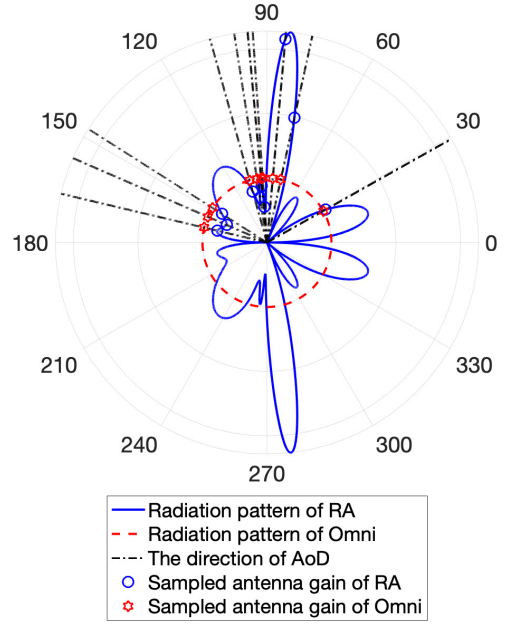


Fig. 2: The radiation pattern for the single-pattern case,  $N_t = 32$ ,  $N_r = 8$ ,  $N_{cl} = 10$ ,  $N_{ray} = 1$ .

## V. SIMULATION RESULTS

Numerical results based on Monte Carlo simulations are presented in this section. We consider the multi-path channel model in (2). Considering the scattering structure of the wireless environment, (2) can be expanded into

$$\mathbf{H} = \sum_{i=1}^{N_{cl}} \sum_{j=1}^{N_{ray}} \alpha_{i,j} \mathbf{a}_R(\theta_{i,j}) \mathbf{a}_T^H(\varphi_{i,j}). \quad (47)$$

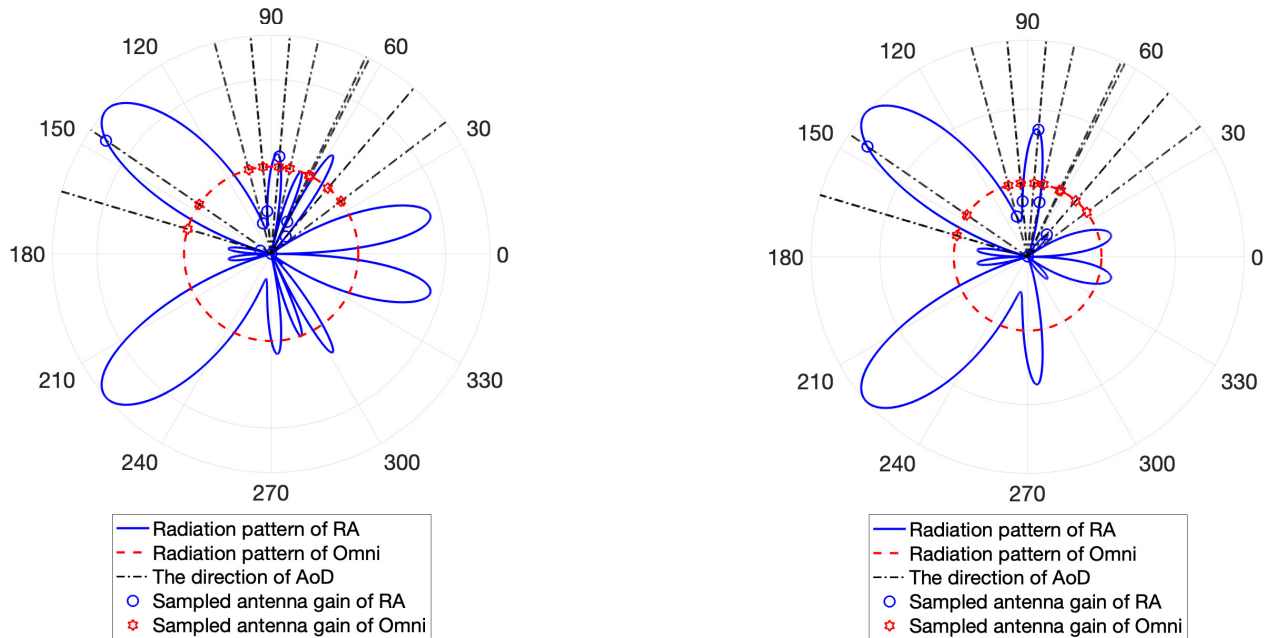
The complex path gain  $\alpha_{i,j}$  are i.i.d.  $\mathcal{CN}(0, \sigma_i^2)$ , where  $\sigma_i^2$  denotes the average power of the  $i$ -th cluster with  $\sum_{i=1}^{N_{cl}} \sigma_i^2 = \gamma$ , where  $\gamma$  is the normalization parameter to ensure that  $\mathbb{E}\{\|\mathbf{H}\|_F^2\} = N_r N_t$ .  $\theta_{i,l}$  is uniformly distributed with mean  $\theta_i$  and a standard deviation  $\xi$ , and  $\varphi_{i,l}$  is uniformly distributed with mean  $\varphi_i$  and the same standard deviation  $\xi$ . All the results are obtained by averaging over 1000 randomly generated channel realizations. Unless otherwise stated,  $N_t = 32$ ,  $N_r = 8$ ,  $\xi = 15^\circ$ , and the half-wavelength antenna spacing is considered for both the transmitter and the receiver. Both  $\theta_i$  and  $\varphi_i$  are uniformly distributed in the range of  $[-\pi/2, \pi/2]$ .

### A. Radiation Pattern

In this subsection, the radiation patterns for both of the single-pattern and the multi-pattern cases are presented via numerical interpolation based on the optimized pattern sampling matrices.

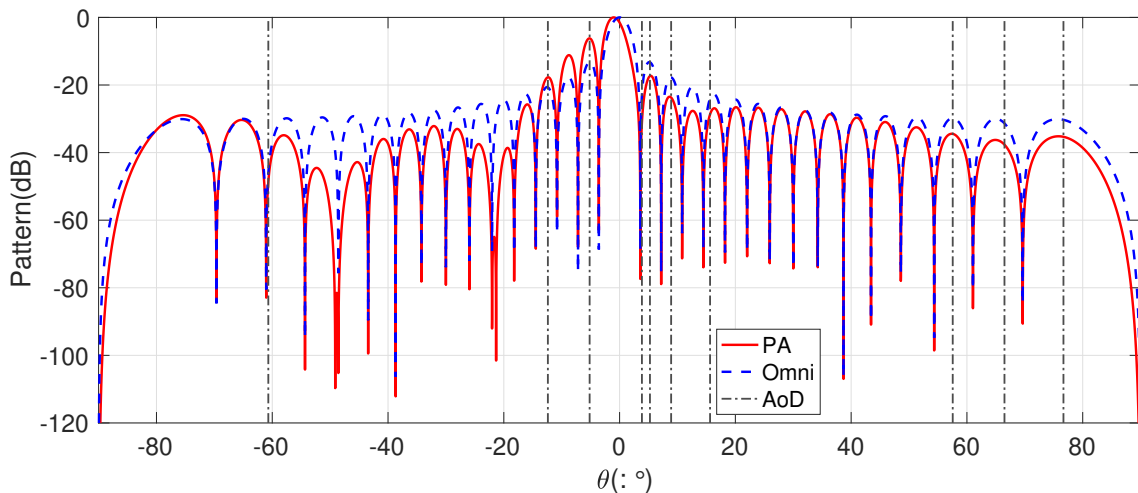
For convenience, the following abbreviations are used throughout this subsection:

- 1) 'RA': the designed reconfigurable antenna.
- 2) 'Omni': the omni antenna or the phased array equipped with omni antennas.



(a) The radiation pattern of Transmit antenna 1

(b) The radiation pattern of Transmit antenna 2

Fig. 3: The radiation pattern for the multi-pattern case,  $N_t = 32$ ,  $N_r = 8$ ,  $N_{cl} = 10$ ,  $N_{ray} = 1$ .Fig. 4: The array radiation pattern v.s. the scanning angle in the single-pattern case,  $N_t = 32$ ,  $N_r = 8$ ,  $N_{cl} = 10$ ,  $N_{ray} = 1$ .

- 3) ‘PA’: the array radiation pattern in the single-pattern system obtained by the power allocation (PA) scheme.
- 4) ‘SOF’: the array radiation pattern in the multi-pattern system obtained by the sequential optimization framework (SOF) scheme.

Through comparing the radiation patterns of reconfigurable and omni antennas in Fig. 2, we can realize the pattern reshaping after reconfigure operation. The sampling values of the pattern in the AoD directions are marked. The redistribution of the antenna gain is realized. We can observe that in a densely scattering region, the antenna gain will be limited for the high

correlation, which is consistent with our design principle. In Fig. 3, we further present the radiation patterns of different RAs in the multi-pattern system. Comparing Fig. 3(a) and Fig. 3(b), we can observe that the correlation modification process results in different patterns on each antenna element. It is worth mentioning that the radiation pattern we designed only optimizes the antenna gain in the direction of AoD because the reconfigurable pattern affects the channel in the AoD directions when the pattern reconfigurability is only considered at the transmitter according to (16). What’s more, EoD and EoA default to  $180^\circ$  to show the directionality of the resulting pattern.

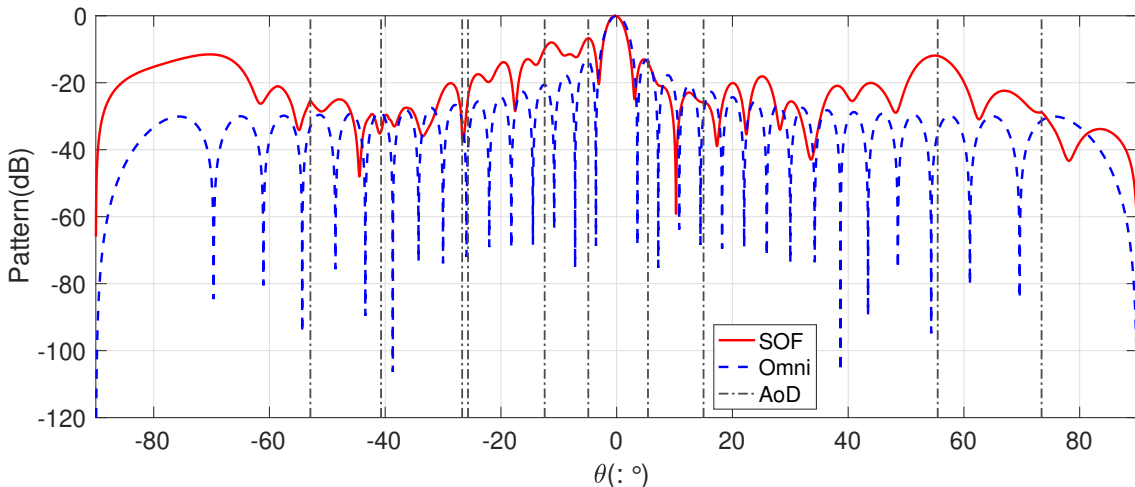


Fig. 5: The array radiation pattern v.s. the scanning angle in the multi-pattern case,  $N_t = 32$ ,  $N_r = 8$ ,  $N_{cl} = 10$ ,  $N_{ray} = 1$ .

Fig. 4 and Fig. 5 present the array radiation pattern of MR-MIMO in the single-pattern and the multi-pattern cases, respectively. When each antenna element has the same pattern, the effect of the phase scanning still exists, compared with the traditional MIMO. The influence of reconfigurable antennas focuses on the redistribution of the scanning power. From Fig. 5, we can observe that the phase scanning effect is destructed by the variety of patterns. What's more, the average power of scattering paths increases compared with the traditional MIMO for the ideal correlation structure obtained by SOF.

### B. Capacity

The numerical results of the system capacity are presented in this subsection. For the good-conditioned channel in the following part,  $\{\sigma_i^2\}$  follows the normal distribution so that the channel condition number will be small. While for the ill-conditioned channel, we set  $\sigma_1^2 : \sigma_2^2 : \sigma_3^2 : \sigma_4^2 : \dots : \sigma_{N_{cl}}^2 = 100 : 50 : 50 : 1 : \dots : 1$  to obtain an extremely uneven distribution of  $\{\sigma_i^2\}$  and the condition number of the ill-conditioned channel matrix is large. The following abbreviations are used throughout this subsection:

- 1) 'Upper Bound': we adopt the ideal channel  $\mathbf{H}_{opt} = \sqrt{N_t} \mathbf{I}_{N_r \times N_t}$ , considering that the eigenvectors of  $\mathbf{H}_{opt}$  have no influence on the capacity calculation, according to (10). Note that this upper bound is generally not achievable in practice.
- 2) 'EOPA': the proposed pattern design scheme in the single-pattern MR-MIMO using the eigenvalue optimization based power allocation (EOPA) scheme.
- 3) 'SDR': the suboptimal scheme in the single-pattern MR-MIMO using the SDR algorithm through Gaussian approximation [35].
- 4) 'SOF-EVD-EOPA': the proposed pattern design scheme in the multi-pattern MR-MIMO using the eigenvalue decomposition-based (EVD-based) SOF with EOPA.
- 5) 'SOF-MO-EOPA': the proposed pattern design scheme in the multi-pattern MR-MIMO using the manifold optimization-based (MO-based) SOF with EOPA.

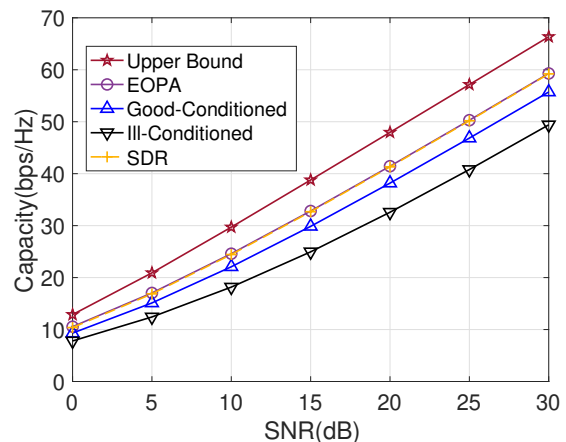


Fig. 6: Capacity v.s. transmit SNR,  $N_t = 32$ ,  $N_r = 8$ ,  $N_{cl} = 10$ ,  $N_{ray} = 8$ , good-conditioned and ill-conditioned channels.

- 6) 'Good-Conditioned': the channel without the pattern reconfigurable antennas. The average power of each cluster has the same value.
- 7) 'Ill-Conditioned': the channel without the pattern reconfigurable antennas. The distribution of each cluster's average power is not even.

In Fig. 6, the performance of EOPA is shown compared with the upper bound with the ideal channel, the suboptimal solution obtained by the SDR with Gaussian approximation, and the physical channel equipped with omni-antennas both in good condition and in ill condition. We can see that the performance of EOPA and SDR can provide a performance gain compared with the physical channel, which shows their superiority. Meanwhile, there is still a gap between the proposed pattern design schemes and the upper bound, which reveals that the lackness of phase modification ability limits the performance of the transmit reconfigurable pattern MIMO.

In Fig. 7, the performance of SOF and EOPA are presented compared with the upper bound, the physical channel in good

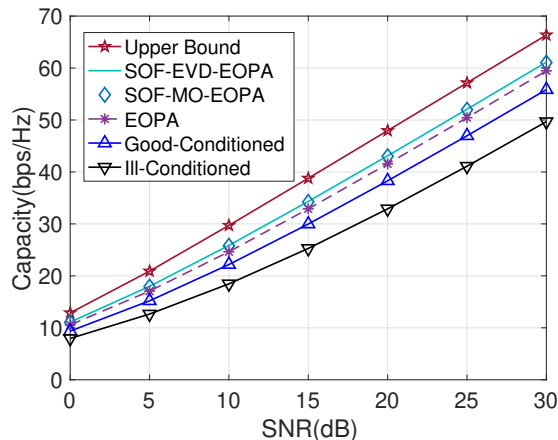


Fig. 7: Capacity v.s. transmit SNR,  $N_t = 32$ ,  $N_r = 8$ ,  $N_{cl} = 10$ ,  $N_{ray} = 8$ , good-conditioned and ill-conditioned channels.

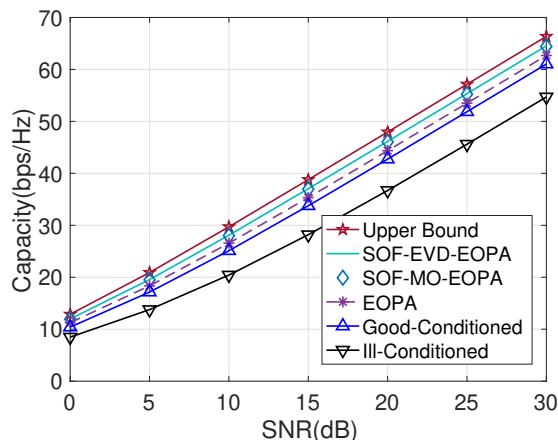


Fig. 8: Capacity v.s. transmit SNR,  $N_t = 32$ ,  $N_r = 8$ ,  $N_{cl} = 20$ ,  $N_{ray} = 8$ , good-conditioned and ill-conditioned channels.

condition and in ill condition when  $N_{cl} = 10$ . On one hand, in the single-pattern MR-MIMO, EOPA can provide a large performance gain especially when the physical channel is bad. However, EOPA can not change the correlation structure of the channel, so the improvement compared with the good-conditioned channel is not apparent. On the other hand, in the multi-pattern MR-MIMO, the quality of the channel can be significantly improved by the correlation modification so that SOF can further improve the performance of EOPA and achieve a significant performance gain. The property is helpful in MIMO system design. With the pattern modification, the ill-conditioned channel will be transformed into good-conditioned.

Fig. 8 shows the analogous simulation results of Fig. 7 when  $N_{cl} = 20$ . Compared with Fig. 7, the achievable capacity of the physical channel in good condition is better for the additional subchannels. Moreover, the performance gap between the modified channel using SOF and the ideal channel becomes smaller, which shows that the modification ability is proportional to the number of clusters. Meanwhile, more scattering paths provide more independent subpaths so that the

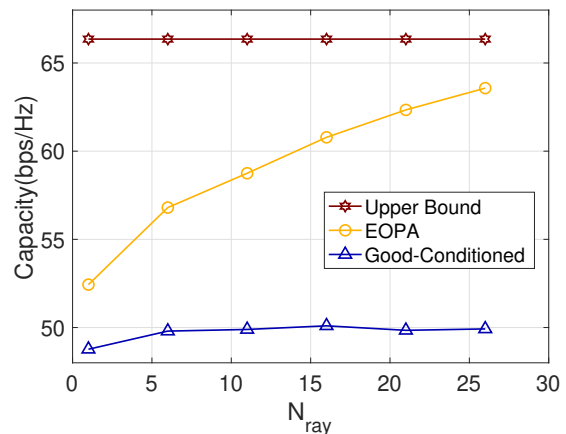


Fig. 9: Capacity v.s. number of rays in each cluster,  $N_t = 32$ ,  $N_r = 8$ ,  $N_{cl} = 10$ ,  $\xi = 3^\circ$ , SNR=30dB, good-conditioned channel.

gap between SOF and EOPA becomes slighter. Finally, SOF-EVD-EOPA and SOF-MO-EOPA have similar performance.

Fig. 9 plots the performance of EOPA in terms of the number of rays  $N_{ray}$  in each cluster when  $N_{cl} = 10$  and SNR=30dB. With the increasing of  $N_{ray}$ , the performance of EOPA is getting close to the upper bound, which reveals that the increased subchannels provide additional degrees of freedom so that the power redistribution ability of EOPA is enhanced. What's more, as the number of subchannels is large enough, the extra contribution due to EOPA is getting marginal so that the slope is decreasing.

## VI. CONCLUSIONS

In this paper, we study the capacity maximization pattern design for MR-MIMO systems. We show that the effect of radiation reconfigurability can be regarded as an additional gain on the corresponding propagation directions. Based on that, the optimization problem of the optimal pattern design is formulated. We further discuss the single-pattern case where the optimized radiation pattern is the same for all the antenna elements, and the multi-pattern case where each antenna element can adopt different radiation patterns. More specifically, the pattern design in the single-pattern case is equivalent to a power redistribution among all scattering paths, and an eigenvalue optimization based power allocation algorithm is proposed. Compared with the single-pattern case, the multiple patterns in the multi-pattern case further offer the freedom of adjusting the correlation structure of the channel. A sequential optimization framework with manifold optimization and eigenvalue decomposition is proposed to obtain near-optimal solutions in the multi-pattern case. Numerical results validate the superiority of MR-MIMO over traditional MIMO systems as well as the effectiveness of proposed algorithms. Our future work includes the application of symbol-level precoding in MR-MIMO systems.

APPENDIX  
PROOF OF PROPOSITION 2

Based on (32), the constraint  $\|\widehat{\mathbf{H}}_i\|_F^2$  can be transformed into

$$\begin{aligned} \|\widehat{\mathbf{H}}_i\|_F^2 &= \text{Tr} \left( \widehat{\mathbf{H}}_i^H \widehat{\mathbf{H}}_i \right) \\ &= \text{Tr} \left( (\mathbf{a}_{T,i} \odot \widehat{\mathbf{m}}_i) \mathbf{a}_{R,i}^H \mathbf{a}_{R,i} (\mathbf{a}_{T,i} \odot \widehat{\mathbf{m}}_i)^H \right) \quad (48) \\ &= \frac{1}{N_t} \sum_{j=1}^{N_t} \widehat{m}_{i,j}^2 = \frac{1}{N_t} \|\widehat{\mathbf{m}}_i\|_2^2, \end{aligned}$$

where  $\mathbf{a}_{R,i}^H \mathbf{a}_{R,i} = 1$  and  $\widehat{m}_{i,j}$  denotes the  $j$ -th element of  $\widehat{\mathbf{m}}_i$ . Based on (48), the equivalence between  $\|\widehat{\mathbf{H}}_i\|_F^2 = 1$  and  $\|\widehat{\mathbf{m}}_i\|_2^2 = N_t$  is proved.

REFERENCES

- [1] L. Zheng and D. N. C. Tse, "Diversity and Multiplexing: A Fundamental Tradeoff in Multiple-Antenna Channels," *IEEE Transactions on Information Theory*, vol. 49, no. 5, pp. 1073–1096, 2003.
- [2] C. Rhee, Y. Kim, T. Park, S.-s. Kwoun, B. Mun, B. Lee, and C. Jung, "Pattern-Reconfigurable MIMO Antenna for High Isolation and Low Correlation," *IEEE Antennas and Wireless Propagation Letters*, vol. 13, pp. 1373–1376, 2014.
- [3] S. Elgiddawy, H. A. Malhat, S. H. Zainud-Deen, A. A. Ibrahim, and H. Hamed, "Compact Reconfigurable Polarization Plasma Square Microstrip Patch MIMO Antenna for 5G Wireless Applications," in *2021 38th National Radio Science Conference (NRSC)*, vol. 1, 2021, pp. 88–95.
- [4] P. Sanchez-Olivares and J. Masa-Campos, "Mechanically Reconfigurable Conformal Array Antenna Fed by Radial Waveguide Divider With Tuning Screws," *IEEE Transactions on Antennas and Propagation*, vol. 65, no. 9, pp. 4886–4890, 2017.
- [5] B. A. Cetiner, E. Akay, E. Sengul, and E. Ayanoglu, "A MIMO System with Multifunctional Reconfigurable Antennas," *IEEE Antennas and Wireless Propagation Letters*, vol. 5, pp. 463–466, 2006.
- [6] N. Ojaroudi Parchin, H. Jahanbakhsh Basherlou, Y. I. Al-Yasir, A. M Abdulkhaleq, and R. A. Abd-Alhameed, "Reconfigurable Antennas: Switching Techniques—A Survey," *Electronics*, vol. 9, no. 2, p. 336, 2020.
- [7] B. He and H. Jafarkhani, "Low-Complexity Reconfigurable MIMO for Millimeter Wave Communications," *IEEE Transactions on Communications*, vol. 66, no. 11, pp. 5278–5291, 2018.
- [8] P. N. Vasileiou, K. Maliatsos, E. D. Thomatos, and A. G. Kanatas, "Reconfigurable Orthonormal Basis Patterns Using ESPAR Antennas," *IEEE Antennas and Wireless Propagation Letters*, vol. 12, pp. 448–451, 2013.
- [9] A. Li, C. Masouros, and C. B. Papadias, "MIMO Transmission for Single-Fed ESPAR With Quantized Loads," *IEEE Transactions on Communications*, vol. 65, no. 7, pp. 2863–2876, 2017.
- [10] N. Ojaroudi Parchin, H. Jahanbakhsh Basherlou, Y. I. Al-Yasir, R. A. Abd-Alhameed, A. M. Abdulkhaleq, and J. M. Noras, "Recent Developments of Reconfigurable Antennas for Current And Future Wireless Communication Systems," *Electronics*, vol. 8, no. 2, p. 128, 2019.
- [11] Y.-F. Cheng, X. Ding, B.-Z. Wang, and W. Shao, "An Azimuth-Pattern-Reconfigurable Antenna With Enhanced Gain and Front-to-Back Ratio," *IEEE Antennas and Wireless Propagation Letters*, vol. 16, pp. 2303–2306, 2017.
- [12] M.-I. Lai, T.-Y. Wu, J.-C. Hsieh, C.-H. Wang, and S.-K. Jeng, "Compact Switched-Beam Antenna Employing a Four-Element Slot Antenna Array for Digital Home Applications," *IEEE Transactions on Antennas and Propagation*, vol. 56, no. 9, pp. 2929–2936, 2008.
- [13] A. Pal, A. Mehta, D. Mirshekar-Syahkal, and H. Nakano, "A Twelve-Beam Steering Low-Profile Patch Antenna With Shorting Vias for Vehicular Applications," *IEEE Transactions on Antennas and Propagation*, vol. 65, no. 8, pp. 3905–3912, 2017.
- [14] J.-S. Row and C.-W. Tsai, "Pattern Reconfigurable Antenna Array With Circular Polarization," *IEEE Transactions on Antennas and Propagation*, vol. 64, no. 4, pp. 1525–1530, 2016.
- [15] Y. Tawk, J. Costantine, and C. G. Christodoulou, "An Eight-Element Reconfigurable Diversity Dipole System," *IEEE Transactions on Antennas and Propagation*, vol. 66, no. 2, pp. 572–581, 2017.
- [16] Y. Zhou, R. S. Adve, and S. V. Hum, "Design and Evaluation of Pattern Reconfigurable Antennas for MIMO Applications," *IEEE Transactions on Antennas and Propagation*, vol. 62, no. 3, pp. 1084–1092, 2013.
- [17] N. Nguyen-Trong, L. Hall, and C. Fumeaux, "A Frequency- and Pattern-Reconfigurable Center-Shorted Microstrip Antenna," *IEEE Antennas and Wireless Propagation Letters*, vol. 15, pp. 1955–1958, 2016.
- [18] N. H. Chamok, M. H. Yilmaz, H. Arslan, and M. Ali, "High-Gain Pattern Reconfigurable MIMO Antenna Array for Wireless Handheld Terminals," *IEEE Transactions on Antennas and Propagation*, vol. 64, no. 10, pp. 4306–4315, 2016.
- [19] Y. I. Abdullaheem, A. S. Abdullah, H. J. Mohammed, B. A. Mohammed, and R. A. Abd-Alhameed, "Design of Radiation Pattern-Reconfigurable 60-GHz Antenna for 5G Applications," 2014.
- [20] M. Hasan, I. Bahceci, and B. A. Cetiner, "Downlink Multi-User MIMO Transmission for Radiation Pattern Reconfigurable Antenna Systems," *IEEE Transactions on Wireless Communications*, vol. 17, no. 10, pp. 6448–6463, 2018.
- [21] A. C. Gurbuz, R. Mdrafi, and B. A. Cetiner, "Cognitive Radar Target Detection and Tracking With Multifunctional Reconfigurable Antennas," *IEEE Aerospace and Electronic Systems Magazine*, vol. 35, no. 6, pp. 64–76, 2020.
- [22] E. Kaderli, İ. Bahçeci, K. M. Kaplan, and B. A. Cetiner, "On The Use of Reconfigurable Antenna Arrays for DoA Estimation of Correlated Signals," in *2016 IEEE Radar Conference (RadarConf)*, 2016, pp. 1–5.
- [23] A. C. Gurbuz and B. Cetiner, "Multifunctional Reconfigurable Antennas for Cognitive Radars," in *2018 IEEE Radar Conference (RadarConf18)*, 2018, pp. 1510–1515.
- [24] I. Bahceci, M. Hasan, T. M. Duman, and B. A. Cetiner, "Efficient Channel Estimation for Reconfigurable MIMO Antennas: Training Techniques and Performance Analysis," *IEEE Transactions on Wireless Communications*, vol. 16, no. 1, pp. 565–580, 2016.
- [25] R. S. Sutton and A. G. Barto, *Reinforcement Learning: An Introduction*. MIT press, 2018.
- [26] N. Gulati and K. R. Dandekar, "Learning State Selection for Reconfigurable Antennas: A Multi-Armed Bandit Approach," *IEEE Transactions on Antennas and Propagation*, vol. 62, no. 3, pp. 1027–1038, 2013.
- [27] T. Zhao, M. Li, and G. Ditzler, "Online Reconfigurable Antenna State Selection Based on Thompson Sampling," in *2019 International Conference on Computing, Networking and Communications (ICNC)*, 2019, pp. 888–893.
- [28] T. Zhao, M. Li, and M. Poloczek, "Fast Reconfigurable Antenna State Selection with Hierarchical Thompson Sampling," in *ICC 2019-2019 IEEE International Conference on Communications (ICC)*, 2019, pp. 1–6.
- [29] T. Zhao, M. Li, and Y. Pan, "Online Learning Based Reconfigurable Antenna Mode Selection Exploiting Channel Correlation," *IEEE Transactions on Wireless Communications*, 2021.
- [30] S. Burer, K. M. Anstreicher, and M. Dür, "The Difference Between  $5 \times 5$  Doubly Nonnegative and Completely Positive Matrices," *Linear Algebra and its Applications*, vol. 431, no. 9, pp. 1539–1552, 2009.
- [31] S. Boyd, S. P. Boyd, and L. Vandenberghe, *Convex optimization*. Cambridge university press, 2004.
- [32] P.-A. Absil, R. Mahony, and R. Sepulchre, *Optimization Algorithms on Matrix Manifolds*. Princeton University Press, 2009.
- [33] J. M. Lee, "Smooth Manifolds," in *Introduction to Smooth Manifolds*. Springer, 2013, pp. 1–31.
- [34] R. A. Horn and C. R. Johnson, *Matrix Analysis*. Cambridge university press, 2012.
- [35] Z.-Q. Luo, W.-K. Ma, A. M.-C. So, Y. Ye, and S. Zhang, "Semidefinite Relaxation of Quadratic Optimization Problems," *IEEE Signal Processing Magazine*, vol. 27, no. 3, pp. 20–34, 2010.